Exploring the stability and electronic properties of Zn-doped hematite surfaces for Photoelectrochemical water splitting

Joseph Simfukwe[1, 2*], Refilwe Edwin Mapasha[1], Artur Braun[3] and Mmantsae Diale[1]

[1]*Physics Department, University of Pretoria, Pretoria 0002, South Africa*

[2]*Physics Department, Copperbelt University, Riverside, Kitwe 10101, Zambia*

[3]*Laboratory for High Performance Ceramics, Emp, Swiss Federal Laboratories for Materials Science and Technology, CH -8600 Dübendorf, Switzerland*

Highlights

• Zinc (Zn) doped {0001} and {01 $\bar{1}$ 2} hematite surfaces are thermodynamically stable and the stability increases with increasing concentration of Zn atoms.
•Mono-doping of Zinc on the topmost layer L1 structure of the {0001} α-Fe_2O_3 surface, decreases the band gap without impurity states in the band structure leading to improved photoelectrochemical (PEC) water splitting.
•Increasing Zinc doping concentration to 4.20% on L1 of {0001} surface, shifts the conduction band minimum (CBM) upwards by 0.23 eV as compared to the bulk.
•In surface doping the photo generated charge carriers can efficiently diffuse to the surface for enhanced interfacial charge transfer to the adsorbates for improved PEC water splitting in hematite.

Corresponding author: Joseph Simfukwe
Email: josephsimfukwe2013@gmail.com
Tel: +27640624781 / +260955958573

Abstract:

First-principles calculations of Zinc (Zn) doped {0001} and {01 $\bar{1}$ 2} hematite surfaces for improved photoelectrochemical water splitting have been studied. The single Zn-doped systems were found to be energetically favourable (negative formation energies) and the stability increased with increasing concentration of Zn atoms. Our results show that even with mono-doping of Zn on the topmost layer L1 structure of the {0001} α-Fe_2O_3 surface, the band gap can be decreased without impurity states in the band structure which normally acts as recombination centres. At the doping concentration of 4.20% of Zn atoms on L1 of {0001} surface, the conduction band minimum (CBM) is shifted upwards by 0.23 eV as compared to the bulk. In addition to the decrease in the band gap, the CBM of the single doped layer 2 (DL21) and layer 3 (DL31) of the {01 $\bar{1}$ 2} surface become wavier and delocalised suggesting improved electron mobility of hematite surface. Charge density difference plots and Bader charge analysis showed the accumulation of charge at the top of the surface with more pronounced charge depleting from Zn atom and accumulating on O and Fe neighbouring atoms, implying that the photo generated charge carriers can efficiently diffuse to the surface for enhanced interfacial charge transfer to the adsorbates. The electronic properties exhibited by doping of Zn on the two hematite surfaces postulate that surface doping is likely to strengthen the electrocatalytic activity of hematite for water splitting.

Keywords: hematite (α-Fe_2O_3); surfaces; Zinc (Zn); photoelectrochemical; band gap

1. Introduction

The realization that fossil fuels are a finite resource, and detrimental to the environment when combusted, has brought about a shift towards more environmentally friendly, renewable energy sources such as photovoltaics (PV), solar thermal, solar fuels and water splitting (WS) in photoelectrochemical (PEC) cells [1]. The principle of a PEC for solar water splitting works as follows: the photoelectrode is dipped into an aqueous electrolyte and exposed to sunlight. A counter electrode is also dipped in the electrolyte and electrically connected with the photoelectrode via a conductor or via a power source, which provides an electric bias. The photoelectrode has a dual function: first, it is a light absorbing semiconductor (SC), which absorbs the photons from sunlight, which in turn produce electron-hole pairs in the volume of the photoelectrode. The holes or electrons are charge carriers, which are expected to diffuse to the surface of a photoelectrode where they perform chemical work. For a photoanode in water, for example, the holes diffuse to the electrode-electrolyte interface, where they should oxidize the water molecule. The electrons in turn diffuse to the backside of the photoelectrode, to the current collector, which can be a transparent conducting metal oxide (TCO) such as fluorine doped tin oxide (FTO). This absorber function can be further tuned by doping (defect engineering) with other elements or by heterostructuring. At large, it is the volume which accounts for the yield of necessary charge carriers. The other function of the photoelectrode is its electrocatalytic activity at the electrode-electrolyte interface, which too can be manipulated by doping and heterostructuring. At the photoanode, the water molecule is oxidized and oxygen (O_2) evolves as gas. The solar fuel hydrogen (H_2) then evolves at the counter electrode.

A semiconducting material is considered good as a photoelectrode for PEC water splitting if it possesses the following qualities: an appropriate band gap that can absorb a larger portion of solar radiation, corrosion stability in aqueous environment, abundant and cost effective. It should also be non-toxic and have a well-positioned conduction band edge (CBE) for direct redox reaction of hydrogen. Hematite (α-Fe_2O_3) is insofar a SC of interest because it satisfies a number of the above stated qualities. It has a band gap of 1.9~2.2 eV [2-4] enabling it to capture ~40% of the solar spectrum, high stability in most electrolyte at pH > 3 [5] and it is low cost [4, 6]. Its solar to hydrogen efficiency is around 15% [7, 8]. Nonetheless, α-Fe_2O_3 inherently suffers from low surface reaction rates [4, 9, 10], poor conductivity [4, 8, 10, 11], low carrier mobility ($< 1\ cm^2\ V^{-1}\ s^{-1}$) [2, 9, 10, 12], quick recombination rates of electron-hole pairs (~10 ps) [4, 8, 9, 13], and a short hole diffusion length (2-4 nm) [4, 8-10]. In addition, while the valence band edge (VBE) of α-Fe_2O_3 is suitably positioned for water oxidation, the energy of the CBE is lower than the hydrogen evolution potential [14, 15]. Hence an external electric bias is required to produce hydrogen at the cathode. Owing to the advantages of α-Fe_2O_3 over other materials, much attention has been paid to overcoming its shortfalls and making it an effective photoelectrode for PEC water splitting to produce clean solar hydrogen energy on a commercial scale.

PEC performance of α-Fe_2O_3 can be improved through doping [4, 5, 15-19], surface treatment [6, 11] and formation of heterojunction between α-Fe_2O_3 and other SCs [11, 20, 21]. Doping preferably over the entire volume increases the donor concentration bringing about increased conductivity and prolongs photo-generated electron-hole pair recombination [11]. However, negative effects of different modes of doping, such as formation of localized impurity states within the band gap which act as recombination centres for the photogenerated charge carriers have been reported [19, 22, 23]. Chang and Liu [24], experimentally studied the photocatalytic performance of vanadium (V) doped surface and bulk titanium dioxide (TiO_2). They found that impurity states of V^{3+}/V^{4+} formed inside the bulk trapped the photo generated holes-electrons which quickly recombined before they could diffuse to the surface, where they are required for interfacial transfer. This significantly reduced the photocatalytic activity of the

bulk doped TiO_2. On the other hand, presence of V^{3+}/V^{4+} on the surface lattice increased the number of trapped holes and facilitated the interfacial charge transfer from the photoactivated TiO_2 to the adsorbates. They concluded that doping on the surface was advantageous in comparison to bulk doping, as it enabled most of the charge carriers to successfully move from inside to the surface and undergo interfacial transfer to the adsorbate. Therefore, with the right mode of doping we can improve the PEC performance of α-Fe_2O_3 for water splitting.

A number of experimental investigations on doping of bulk α-Fe_2O_3 with Zn to improve the photo activity have been carried out [4, 6, 16, 18, 25]. It is generally reported that Zn doping of α-Fe_2O_3 leads to an improved photocatalytic activity of the system and various reasons and explanations as to the source of the observed improved photocurrent have been given. Kumari *et al.*[18] prepared Zn-doped α-Fe_2O_3 by spray pyrolysis using iron(III)nitrate as a precursor solution. They reported an increase in the flatband potential and a charge carrier depletion layer width at the semiconductor-electrolyte junction as the source of improved photocurrent density. They further observed that, the Zn-doped hematite produced n-type conductivity. On the other hand, Khan *et al.* [16] noticed a p-type conductivity in the Zn-doped α-Fe_2O_3 when they used iron(III)chloride as a precursor solution, but using the same method of preparation. They reported an increase in the photocurrent density, which was attributed to the increase in the acceptor density as a result of doping with Zn. The p-type conductivity of Zn-doped α-Fe_2O_3, was also recently observed by Hsu *et al.*[26]. In their case, a spin-coating method was used to fabricate Zn-doped α-Fe_2O_3 but also used iron chloride as the precursor solution and Zn chloride as an acceptor dopant. They observed a good photocurrent response, enhanced electron-transfer reaction and improved PEC activity at a doping level of 10% as a result of the enhanced light absorption of the Zn-doped hematite. The enhanced absorption was ascribed to the disorder of the α-Fe_2O_3 lattice induced by the Zn dopant. With density functional theory (DFT), we can effectively determine the nature of crystal disorder by examining and measuring the bond lengths of the structure. The differences in the nature (n-type or p-type) of the Zn-doped hematite were attributed to the selection of the precursor solution and the conditions of preparation [18]. Toroker *et al.* [27] argues that p-type dopants at the surface were useful in reducing the over-potential for increasing the efficiency of the catalyst on the surface. Wong *et al.* carried out a surface treatment of hematite photoanode with Zn acetate for water oxidation, using a spin coating method [6]. Their results indicated that a thin zinc oxide (ZnO) overlayer deposited on thin film of α-Fe_2O_3 increased the photocurrent and reduced the onset potential for oxygen evolution from water. However, despite the reported increase in photocurrent of more than 40% as compared to non-treated α-Fe_2O_3, their water splitting efficiency was 0.11% [6]. This is indeed far below the performance of an ideal SC material. Furthermore, Mirbagheri *et al.* [4] argues that reduced onset potential and Zn contribution to surface states improved the photocatalytic performance of Zn-doped hematite.

It is clear that there has been some good experimental work on Zn-doped hematite for PEC WS and also that more work still remains to be done to fully commercialise hematite as an efficient photoelectrode for PEC activity. It is also noted that theoretical investigation on Zn-doped hematite and its surfaces in very limited in literature. Theoretical computer simulations have become important in understanding experimental results and predicting those not yet done experimentally [15, 19, 28]. In this work, we have carried out first-principles calculations of Zn-doped $\{0001\}$ and $\{01\bar{1}2\}$ hematite surfaces to understand the influence of Zn atom on the stability and electronic structure properties of the two surfaces. This is in a quest to finding a better mode of doping in improving the PEC performance of hematite for water splitting. We intend to shed more light on the effects of Zn atom on the $\{0001\}$ and $\{01\bar{1}2\}$ most stable surfaces of hematite using density functional theory (DFT) calculations. We have examined the stability of the two surfaces and the Zn-doped systems and find them to be stable. We also

determined the effect of Zn concentration on the {0001} surface. At the doping concentration of 4.20% of Zn atoms on L1 of {0001} surface, the conduction band minimum (CBM) shifts upwards by 0.23 eV as compared to the bulk. The charge density difference plots and Bader charge analysis are also carried out.

2. Methodology

All calculations were carried out using plane-wave pseudopotential method with quantum-espresso simulation package [29], a first-principles plane wave code based on DFT [30, 31]. The generalized gradient approximation (GGA), of Perdew, Burke and Ernzerhof (PBE) [32] was used to describe the exchange and correlation energies. The interaction between the core and the valence electrons were represented by the Utralsoft Pseudopotential of PBE. The GGA functional tend to under estimate the band gap in semiconductors by under estimating the binding of the Fe 3d electrons [33]. The inclusion of a Hubbard U correction term for the 3d electrons leads to the correct determination of the semiconductor band gap. In this study we used (DFT + U) with U=5 eV, to obtain the correct band gap of α-Fe_2O_3 [34-36]. We tested the variation of the U parameter with the band gap and found a similar trend as that found by Dzade *et al.* [28] , with U=5eV giving us the correct description of the band gap for α-Fe_2O_3 as presented in Fig. 1. The same U=5 eV value was also used by Rohrbach *et al.* [37] and Bandyopadhyay *et al*. [38] and obtained band gaps comparable to experimental values. Interestingly the value of U=5eV also works well for the Zn 3d electrons as was used by Koster *et al*. [33] possibly because both Fe and Zn are 3d elements. The Kohn-Sham equations were expanded using plane-wave basis set with the kinetic energy cut-off of 350 eV. The convergence threshold was 10^{-5} eV for energy and 10^{-2} eV/Å for the force. A vacuum space of 20 Å which worked well in our previous calculation [10] to avoid interactions between the periodic surface slabs was used even in the present calculations. To study the effects of Zn on the stability and electronic structure of the two surfaces, a supercell method was used. The Monkhorst-Pack scheme k-point grids [39] of 6 x 6 x 2 were used in calculating the density of states (DOS) of 120 atoms supercell of each surface.

Fig. 1(a) shows a hexagonal unit cell from which the α-Fe_2O_3 surfaces were constructed. It is noted that along the c-axis, α-Fe_2O_3 is alternately arranged by 12 Fe layers and six (6) O layers as seen in Fig. 1(a), consequently, along the [0001] axis, three different terminating surfaces can be constructed, namely, single Fe-layer (Fe-O_3-Fe-R), double Fe-layers (Fe-Fe-O_3-R) and O-terminating layer (O_3-Fe-Fe-R), where R is the remaining repeating atomic layers in the bulk unit cell [9, 40]. In this study different surfaces were constructed and analyzed by calculating their surface energies. For the full results and formulae used in the calculations of surface energies of the various surface studied the reader is referred to [10], which is our immediate past study. Fig. 1(c) and (d) show the single Fe-terminating surface and the $\{01\,\overline{1}\,2\}$ surface respectively, which we studied in the present work. The Figure also shows Fe layers; L1, L2 and L3 at which the Zn atom was substitutionary doped. These layers were further denoted as DL11, DL21 and DL31, where letter D refers to doped, L is for layer, the first number denotes the layer number and the second number is the number of Zn atoms substituting Fe. Experimental and theoretical studies have shown that the {0001} and $\{01\,\overline{1}\,2\}$ surfaces have the dominate growth faces of natural hematite [28]. It is further observed that of the three different terminating surfaces stated earlier, the single Fe-terminating surface is the most stable structure [40]. We therefore focused on the two surfaces in our current study. Their stability was determined in the previous study [10] and they were found to be thermodynamically stable. Therefore in this study we start by determining the energetic stability of the two surfaces when doped with the Zn atom.

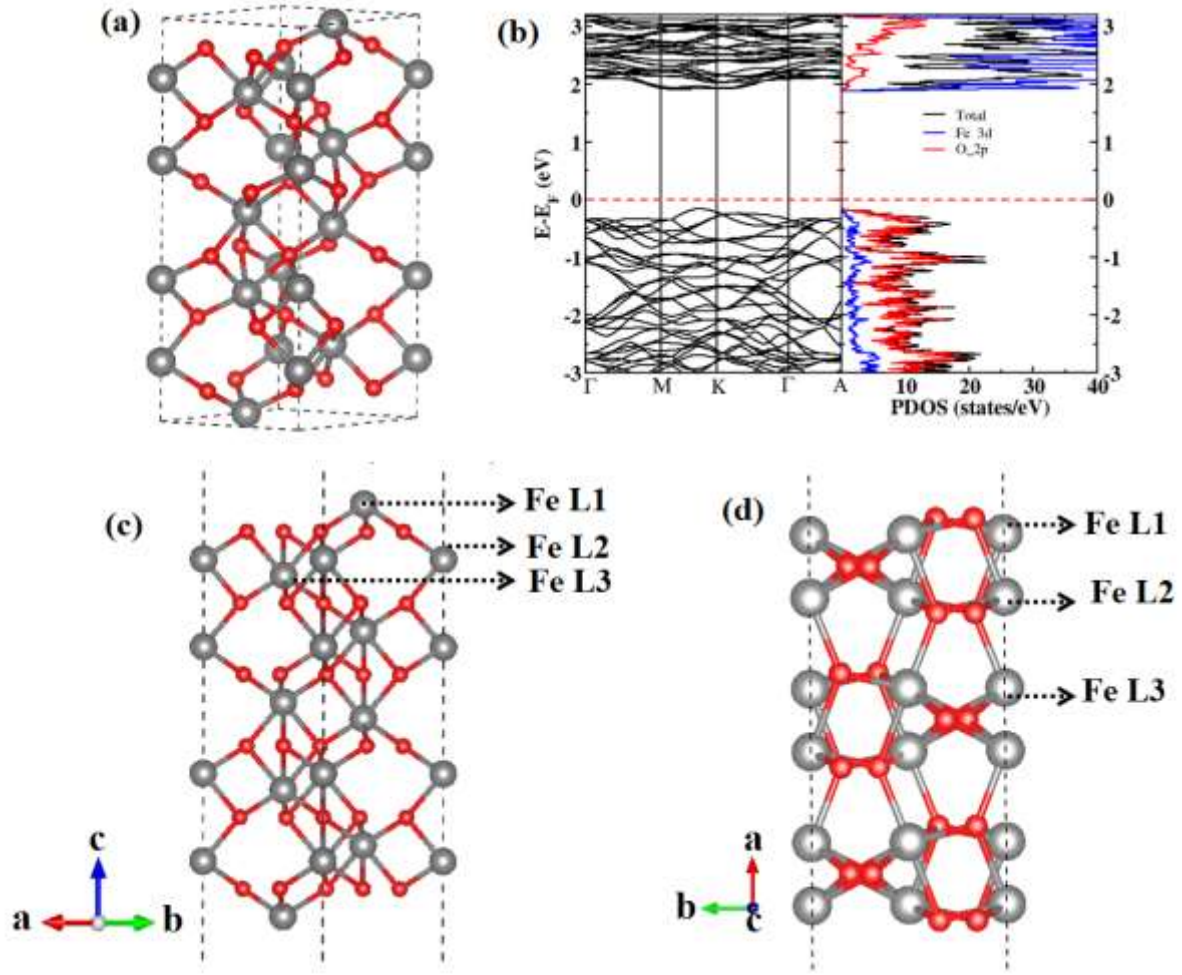

Fig. 1 (a) Hexagonal unit cell of bulk α-Fe_2O_3 (b) the band structure (left), total and partial density of states (PDOS) (right) of pristine bulk α-Fe_2O_3. The Fermi level is set to zero. (c) Single Fe-terminating {0001} surface of hematite (d) $\{01\bar{1}2\}$ surface structure of hematite. Color scheme: Gray (large spheres) and red (small spheres) denotes Fe and O atoms respectively.

3. Results and discussions

Fig. 1 (b) shows the calculated electronic structure of pristine bulk α-Fe_2O_3. It is seen that the valence band maximum (VBM) constitutes of O 2p states and small contribution of Fe 3d states while the CBM is composed of Fe 3d states, in agreement with literature [9, 10, 28]. The DFT+U calculated band gap is 2.1eV while the optimized lattice parameters of pristine hematite are $a = b = 5.00$ Å and $c = 13.85$ Å. Fig. 2 shows the coordination number (CN) of (a) bulk hematite, (b) {0001} surface and (c) $(01\bar{1}2)$ surface. Table 1 presents the Fe-O bond length and CN for the structures shown in Fig. 2. Bulk hematite consists of 3 long Fe-O bond lengths (BL_1) and 3 short Fe-O bond lengths (BL_2), giving a CN of six (6) for each Fe atom. The Fe-O bond lengths of bulk hematite, presented in table 1 compared very well with [10]. When the bulk structure is cut to construct a {0001} and $\{01\bar{1}2\}$ surfaces, there is a reduction in the CN from 6 to 3 and 5 respectively on the top layer L1. The observed changes in the CN of the surfaces also bring about changes in the Fe-O bond lengths. It can be seen from table 1 that for the {0001} surface, there is a reduction in all the 3 Fe-O bond lengths (BL_2) by 0.13 Å from the initial value of 1.93 Å, which seem to be related to the decrease in the CN. This observation is agreement

with Huang *et al.* [41-43] who found that contraction in the surface bond length depended on their CN. They further explained that the bond length becomes stronger with the decrease in the CN, which means that the bond energy may increase with a reduction in CN. We however, observe that for the {01 $\bar{1}$ 2} surface there is both an increase and a decrease in the Fe-O bond lengths. We can see that with the removal of one of the 3 Fe-O bond lengths (BL_1), the remaining two bonds, one decreases by 0.17 Å while the other one increases by 0.02 Å. For the other pair of the 3 Fe-O bond lengths (BL_2), two of them decrease by 0.05 Å and 0.01 Å, while the third one increases by 0.01 Å. Hence, we see a complete different pattern for this structure. This could be attributed to the change in the crystal system from hexagonal system (where $a = b \neq c,\ \alpha = \beta = 90,\ \gamma = 120$) to orthorhombic system (with $a \neq b \neq c,\ \alpha = \beta = \gamma = 90$), where *a*, *b* and *c* are the linear dimensions of the crystal α, β and γ are the interfacial angles. The {0001} surface still remains a hexagonal system. Therefore, we note that the {01 $\bar{1}$ 2} surface does not even follow the concept proposed by Huang *et al.* of the decrease in CN leading to decrease in the bond length because there is both decrease and increase in BLs. In the subsequent inner layer L2, the CN returns to 6 for both surfaces and the Fe-O bond lengths still show some contraction in the {0001} surface as they also share in the stress from the atoms on top, however for the {01 $\bar{1}$ 2} surface there is still some increases and decreases in the Fe-O bond lengths.

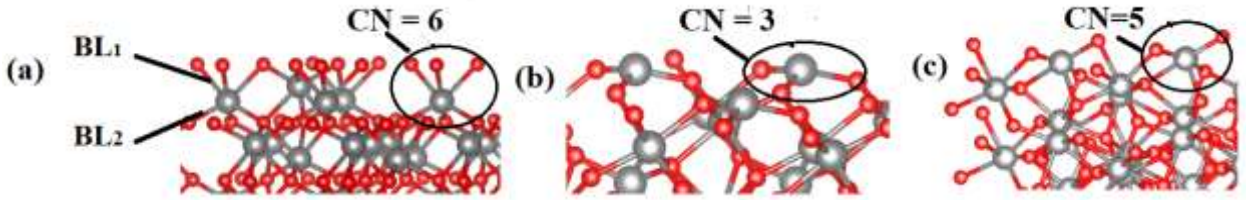

Fig. 2 (a) Longer Fe-O bond length (BL_1), shorter Fe-O bond length (BL_2) and a 6 CN for bulk α-Fe_2O_3 (b) 3 CN for {0001} surface and (c) 5CN of {01 $\bar{1}$ 2}

Table 1. Fe-O bond lengths, coordination number for bulk α-Fe_2O_3, (0001) and (01 $\bar{1}$ 2) Surfaces

Structure	Fe Layer number	Fe-O bond(Å)		CN
Bulk	L1/L2	2.13 x 3 1.93 x 3	(BL_1) (BL_2)	6
(0001) Surface	L1	1.80 x 3	(BL_2)	3
	L2	2.08 x 3 1.98 x 3	(BL_1) (BL_2)	6
(01 $\bar{1}$ 2) Surface	L1	1.96, 2.15 1.88, 1.92, 1.94	(BL_1) (BL_2)	5
	L2	2.17, 2.06, 2.24 2.00, 2.02, 2.06	(BL_1) (BL_2)	6

3.1 Energy of formation for single Zn-doped hematite surfaces

In an attempt to understand the growth conditions in experimental work and the energetic stability of Zn-doped α-Fe_2O_3 surfaces, we calculated the formation energy E_{form} of the Zn-doped surfaces using equation (1) [22, 44].

$$E_{form} = E(Zn\ doped) - E(pure) - n\mu_{Zn} + n\mu_{Fe} \quad (1)$$

where $E(Zn\ doped)$ and $E(pure)$ are the total energies of Zn-doped and pure hematite surfaces respectively. n is the number of Zn atoms in substitution of Fe atoms, whereas μ_{Zn} and μ_{Fe}

stands for the chemical potentials of Zn and Fe atoms respectively. In determining μ_{Fe} and μ_O equation (2) imposes the restrictive conditions [19, 22, 44].

$$2\mu_{Fe}+3\mu_O = \mu_{Fe_2O_3} \quad (2)$$

where $\mu_{Fe_2O_3}$ is the total energy of one formula α-Fe_2O_3. The energy of formation for the doped systems depends upon growth conditions, which varies between the O-rich and Fe-rich. Hence, μ_{Fe} is calculated from the stable bulk α-Fe with one atom for Fe-rich conditions and the corresponding μ_O is obtained using equation (2). Similarly, under O-rich conditions, μ_O is determined from half of the energy of the O_2 molecule and the μ_{Fe} obtained from equation (2). Table 2 presents results of energies of formation for the doped systems. It is noted that E_{form} for one Zn atom substituting Fe atom for the three doped layers DL11, DL21 and DL31, under Fe-rich are positive (endothermic) while under the O-rich they are negative (exothermic) for both surfaces {0001} and {01 $\bar{1}$ 2}. These results indicate that Zn atom substituting Fe atom in the host lattice is a preferred phenomenon. This also implies that Zn doping of hematite under oxygen-rich costs less energy than doping it under Fe-rich conditions. This is an indication that our structures would experimentally prefer to form under the conditions in which the host species surrounds the Zn atom. Furthermore DL11 of {0001} structure shows highest stability under O-rich conditions where as DL21of {01 $\bar{1}$ 2} surface, is the most stable with the highest E_{form} under O-rich condition. We think that these disparities could be ascribed to the differences in the crystal structure systems. The {0001} hexagonal structure has a systematic variation of energy from the top layer L1 to the third inner layer L3 corresponding to the change in the Fe-O bond lengths energy as proposed by Huang *et al* which we alluded to in the earlier discussion. Similarly, as earlier observed, the {01 $\bar{1}$ 2} orthorhombic structure had different variations in the Fe-O bond lengths at each layer, which also translates into a non systematic variation in the E_{form}. However, the DL21 seem to be the most stable structure for this surface.

Table 2: Formation energies of Zn-doped α-Fe_2O_3 surfaces.

		(0001) α-Fe_2O_3 Surface		(01 $\bar{1}$ 2) α-Fe_2O_3 Surface	
	Doped layer	**Fe-rich**	**O-rich**	**Fe-rich**	**O-rich**
E_{form} (eV)	DL11	2.37	**-2.43**	1.98	-2.53
	DL21	3.13	-1.67	1.05	**-3.46**
	DL31	3.16	-1.64	1.36	-3.14

3.2 Formation energies versus Zn concentration on the {0001} α-Fe_2O_3 surface

We further investigated the effect of Zn concentration on the electronic properties of the {0001} surface on the topmost layer L1. This is because DL11 of the {0001} surface showed to be the most stable as compared to the three doped layers. The concentration of Zn was varied according the formula $\alpha - Fe_{2-x}Zn_xO_3$, where $x = 0.021$ for $\alpha - Fe_{47}ZnO_{72}$ (DL11), $x = 0.042$ for $\alpha - Fe_{46}Zn_2O_{72}$ (DL12), $x = 0.063$ for $\alpha - Fe_{45}Zn_3O_{72}$(DL13) and $x = 0.084$ for $\alpha - Fe_{44}Zn_4O_{72}$ (DL14), the doping was done on a 2x2x1 supercell cell surface of hematite with 120 atoms. It is noted that the formation energies with respect to the concentration of Zn atom are negative in O-rich and decrease monotonically. This shows that DL1 remains stable with the

increased number of Zn atoms on the surface and is desirable under O-rich. Table 3 presents the results of E_{form} versus Zn concentration.

Table 3: E_{form} of Zn-doped {0001} hematite structure with respect to concentration.

.	(0001) α-Fe_2O_3 Surface			
E_{form} (eV)	**Doped layer**	**Concentration**	**Fe-rich**	**O-rich**
	DL11	$\alpha - Fe_{47}ZnO_{72}$ (0.021)	2.37	-2.43
	DL12	$\alpha - Fe_{46}Zn_2O_{72}$ (0.042)	3.49	-6.11
	DL13	$\alpha - Fe_{45}Zn_3O_{72}$ (0.063)	4.76	-9.65
	DL14	$\alpha - Fe_{44}Zn_4O_{72}$ (0.084)	6.51	-12.69

3.3 Charge density difference

The charge density difference $(\Delta\rho)$ was plotted using equation (3) to understand the nature of bonding and charge distribution among the atoms.

$$\Delta\rho = \rho_{AB} - \rho_A - \rho_B \quad (3)$$

where ρ_{AB} is the total charge density of the Zn-doped surface, ρ_A and ρ_B are the charge densities of the isolated pure surface and Zn atom respectively. Fig. 3 shows (a) the top and (b) side views of $\Delta\rho$ plots of DL12 of {0001} surfaces. We notice a clear redistribution of electronic charges after doping. Similar to our previous study on Cu doped hematite surfaces [10], the electronic charges are seen to build up at the top of the surface. It is also clearly seen that more charge is depleted from the Zn atom and accumulated on the nearest O and Fe atoms. Quantitative analysis of the Bader charges around each atom reveals that the Zn atom donates 1.27*e* to form bonds with the neighbouring Oxygen atom, while the accepted charge on the Oxygen is found to be -1.18*e* and -0.39*e* on Fe atoms. Therefore as suggested by Chang and Liu [24], the accumulation of electronic charges at the surface may facilitate the facile transfer of charge to the adsorbates and also reduces charge recombination due to the reduced distance to the adsorbate, resulting in enhanced PEC activity of hematite.

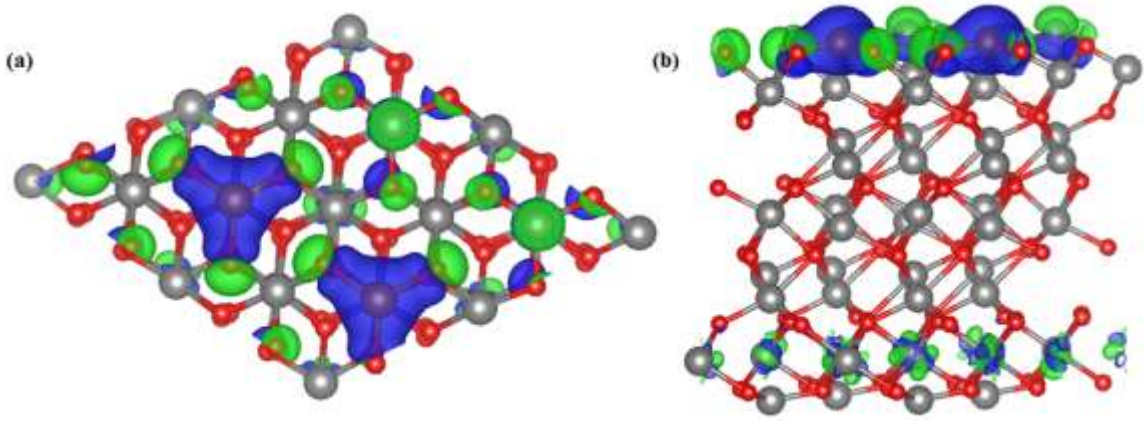

Fig. 3 Charge density difference plots of doped DL12 of {0001} surface calculated at the isosurface value of 0.20electrons/bohr^3 (a) Top and (b) side view. The blue color shows depletion in charge density while the green color shows accumulation in the charge density.

3.4 Electronic properties

Having tested our calculation methods on the pristine bulk hematite and obtained results that are consistent with experimental and previous studies, we now examine the effects of Zn atom on the electronic structure of {0001} and {01 $\bar{1}$ 2} surfaces. Fig. 4 (a) shows the band structure (left) and PDOS (right) of pristine {0001} surface. We notice that just like in the pristine bulk hematite, the VBM constitutes of the O 2p orbital and a small contribution from Fe 3d states while CBM is composed of Fe 3d states. Fig. 4 (b) presents band structure (left), PDOS (right) for DL11, while Fig. 4(c) shows the enlarged PDOS of DL11 for a clear view. Fig. 4 (d) presents band structure (left) and PDOS (right) for DL31. In Fig. 4 (b) and (c) we observe that when Fe atom is substituted by a Zn atom on L1 of {0001} α-Fe_2O_3 surface, a delocalised intermediate band (IB) is introduced just below the Fermi level and the band gap is decreased from ~2.1 eV to 1.90 eV. The IB is contributed by the Fe 3d orbital as revealed by PDOS. Wang *et al.* [22] and Pan *et al.* [45] reported similar observations in the study of (Rh + F) codoped bulk TiO_2 and CrO codoped of GaN respectively. They pointed out that a delocalised IB plays an important role in improving the photocatalytic activity of the doped material by acting as a stepping stone in bridging the VB top and the CB bottom. The electrons excited by the photon energy can easily jump from the VB to the CB via this delocalised IB. Therefore, we note that mono-doping of Zn atom on the topmost layer (L1) of {0001} α-Fe_2O_3 surface can virtually decrease the band gap, leading to increased photon absorption. This also suggests that even with mono-doping of Zn atom on the topmost layer of {0001} α-Fe_2O_3 surface, which is also the most stable structure, we can get similar results to the ones obtained in codoping systems [19, 22, 45]. It is also noted from the PDOS in Fig. 4 (b) and (c) that, the VBM is composed of the Fe 3 d states, Zn 3d states and O 2p states, while the CBM constitutes of Zn 4s states and O 2p states. Furthermore, we observe that as the doping is done slightly down on the inner layers L2 (DL21) and L3 (DL31) of {0001} surfaces, localized acceptor states are induced above the valence band maximum (VBM) and the band gap for DL31 decreases from ~2.1 to 1.71 eV. We only show DL31 in Fig. 4 (d), DL21 had similar features as DL31. Consequently, despite the observed decrease in the band gap of DL21 and DL31, the photocatalytic activity of α-Fe_2O_3 may not improve due to the localization of the states.

Fig. 5 (a) depicts the band structure (left) and PDOS (right) of undoped {01 $\bar{1}$ 2} surface whereas (b), (c) and (d) present band structures (left) and PDOS (right) of DL11, DL21 and DL31 respectively. In Fig. 5 (a) we see a reduction in the band gap of 1.43 eV as compared to 2.1 eV of the bulk. This could be attributed to dangling bonds on the surface due to the change in CN, which introduced gap states that expanded into the band gap. The induced states led to the shifting up and down of the VBM and CBM respectively as can be seen in Fig. 5 (a). This observation was also made by Dzade *et al.* [28] and Li *et al.*[46]. Fig. 5 (b), (c) and (d) show that when Fe atom is replaced by Zn atom on the {01 $\bar{1}$ 2}α-Fe_2O_3 surface, the surface remains semi-conducting while the band gaps of DL11, DL21 and DL31 decrease from 1.43 eV to ~1.0 eV. It is further seen that while localized electronic states are observed in DL11 of the {01 $\bar{1}$ 2} surface as observed in Fig. 4 (b), there are no impurity states formed within the band gaps of DL21 and DL31 as shown in Fig. 5 (c) and (d) respectively. This suggests improved photocatalytic activity of hematite due to the decrease in the band gap and the absence of impurity states in the band structure which often acts as recombination centres. Fig. 5 (c) and (d) shows delocalization and wavy nature of the conduction band minimum (CBM) of DL21 and DL31. Therefore, as observed by Pan *et al.* [19], this could lead to improved carrier mobility in the system, as a result of decreased electron mass. The decreased electron mass is likely to enable the excited electrons to successfully diffuse to the surface and participate in the cathodic

reaction for the evolution of hydrogen on the $\{01\bar{1}2\}$ surface. Also the results show that Zn substituting Fe site is a p-type dopant, in agreement with experimental results of [16, 26]. This can be seen in the position of the acceptor states particularly in Fig. 4 (b), (d) and Fig. 5. (b).

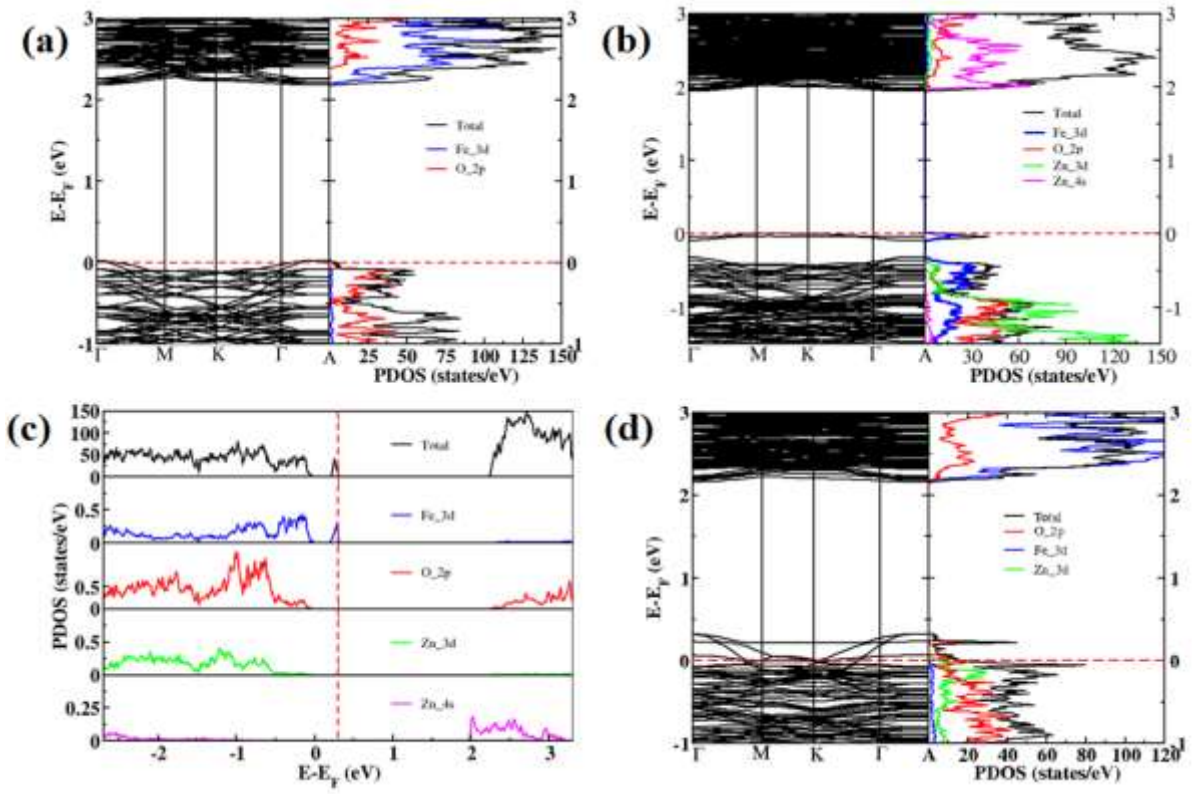

Fig. 4 Band structure and density of states of (a) pure {0001} surface (b) DL11 (c) PDOS of DL11enlarged and (d) DL31. The Fermi level is set to zero

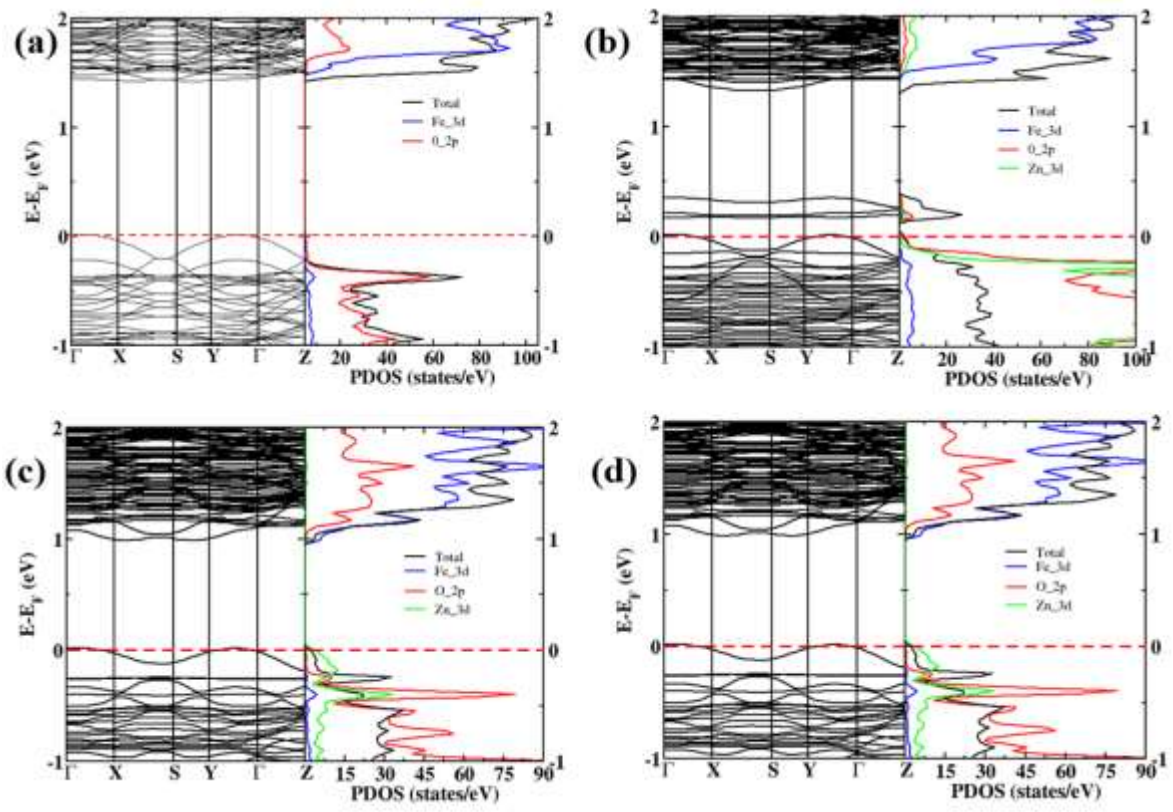

Fig. 5 Band structure and density of states of (a) pure {01 $\bar{1}$ 2} surface (b) DL11 (c) DL21 and (d) DL31. The Fermi level is set to zero

To further understand the effect of Zn concentration on the electronic properties of doped DL1 {0001} surface, the band structures and the PDOS were plotted. Fig. 6 (a) shows the band structure (left) and PDOS (right) of single doped DL11, which we have already discussed and included here for comparison purposes. Fig. 6 (b), (c) and (d) present band structure (left) and PDOS (right) of DL12, DL13 and DL14, the systems doped with two, three and four Zn atoms, which corresponds to doping concentration of 4.20%, 6.30% and 8.33% respectively. It is seen from Fig. 6 that when doping is restricted to the topmost layer of the {0001} surface, impurity states which act as recombination centres are absent. Many researchers [19, 22, 45] have shown that the impurity states can only be eliminated by codoping. However, our results show that even with mono-doping of Zn on the topmost surface DL1, the impurity states can be eliminated. In Fig. 6 (b) it is clearly seen that when DL12 is doped with two (4.20%) Zn atoms the CBM moves slightly upwards to the higher energy level compared to the single (2.10%) doped DL11 (a). It is further noted that the CBM of DL12 is mainly composed of the Fe 3d, O 2p and Zn 4s orbitals, while the VBM is made up of the Zn 3d and O 2p. Further analysis of the band structure reveals that the band gap did not change much compared to the pristine surface but the CBM moved upward by 0.23eV compared to the bulk. In Fig. 6 (c) and (d) we see that the increase in concentration of Zn atoms on DL1 causes the CBM to move downward, leading to the narrowing of the band gap of DL13 and DL14 to 1.71 eV and 1.61 eV respectively. However, the VBM remains unchanged in both cases. In both Fig. 6 (c) and (d), the CBM consists mainly of Zn 4s, O 2p and small portion of Fe 3d orbitals, while the VBM is made up of Zn 3d, O 2p and Fe 3d orbitals. We note that the high presence of the Fe 3d orbital in the CBM of DL12 as compared to DL13 and DL14 may have lead to the up shift of the CBM, while the high composition of Zn 4s and O 2p in the CBM lead to its moving downwards. The decrease in the band gap and the absence of impurity states within the band structure of DL13 and DL14 is likely to improve the PEC activity of hematite due to enhanced absorption of visible light. However, the only

challenge is on the lowering of the CB, which implies an external bias is still needed for the redox reaction to take place. In the case of DL12, the absence of impurity state and the up shift of CBM by 0.23 eV can effectively enhance the PEC performance of the doped hematite surface.

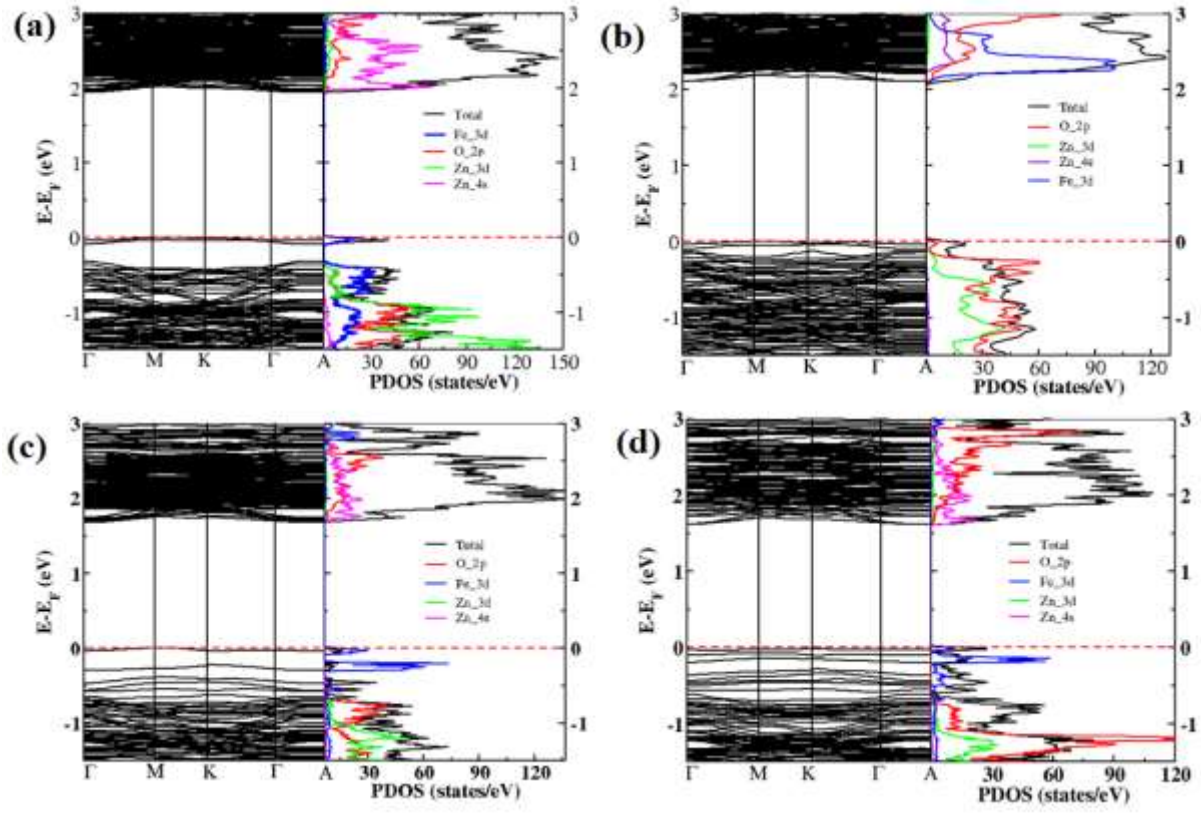

Fig. 6 Band structure and density of states of (a) DL11 (b) DL12 (c) DL13 and (d) DL14. The Fermi level is set to zero

Fig. 7 shows the calculated band edge (VBM and CBM) positions of pure and Zn-doped surfaces of (a) {0001} surface (b) {01 $\bar{1}$ 2} as measured with respect to that of bulk α-Fe_2O_3. The results show that with the cut surfaces of hematite, the CBM of the {0001} surface is shifted upward by 0.27 eV, while the VBM moves up by 0.20 eV but the band gap remains at 2.1 eV. On the other hand, the CBM of {01 $\bar{1}$ 2} surface moves down by 0.48 eV, while the VBM moves up by 0.19 eV leading to decreased band gap of ~1.43 eV as explained earlier. It is further observed that with respect to the pristine bulk hematite, the CBM of DL11, DL21 and DL31 of the {0001} surfaces moves upward by 0.05 eV, 0.16 eV and 0.26 eV, while their VBM are elevated by 0.19 eV, 0.49 eV and 0.53 eV respectively. It is also seen that with respect to the pristine {0001} surface, the CBM of DL11, DL21 and DL31 of the {0001} surfaces moves downward by 0.22 eV, 0.11 eV and 0.01 eV respectively. The VBM of DL11 moves down by 0.01 eV, while the VBM of DL21 and DL31 are elevated by 0.19 eV and 0.33 eV respectively. The upward movement of the VBM leads to a significant decrease in the band gap especially for DL21 and DL31. DL12, DL13 and DL14 are systems with increased concentration of Zn atoms on DL1 of {0001} surface. We see that in all the three systems the VBM moved upwards by 0.19eV with respect to the bulk. Whereas the CBM of DL12 moved upwards by 0.23eV with respect to the bulk, the CBM of DL13 and DL14 moved downward by 0.20eV and 0.29eV respectively, leading to an appreciable decrease in the band gap. In the case of the {01 $\bar{1}$ 2} surface as shown in Figure 6 (b), the CBM of DL11, DL21 and DL31 moves downward by 0.58 eV, 0.78 eV and 0.90 eV, while their VBM are elevated by 0.54 eV, 0.19 eV and 0.19 eV

respectively. On the other hand, with respect to the pristine {01 $\bar{1}$ 2} surface, the CBM of DL11, DL21 and DL31 of the {01 $\bar{1}$ 2} surface moves downward by 0.10 eV, 0.26 eV and 0.42 eV respectively. The VBM of DL11 moves upward by 0.35 eV, while the VBM of DL21 and DL31 remains unchanged at 0.19 eV respectively. The downward movement of the CBM in the {01 $\bar{1}$ 2} surface leads to a significant decrease in the band gap suggesting increased absorption of the photons in the visible light, however, the lower position of the CBM with respect to the pristine bulk hematite which is already low, does not favour the redox reaction without the use of an external bias. Therefore, comparing the two surfaces with the different doping positions, we note that DL1 of the {0001} surface may be more feasible for enhanced PEC water splitting.

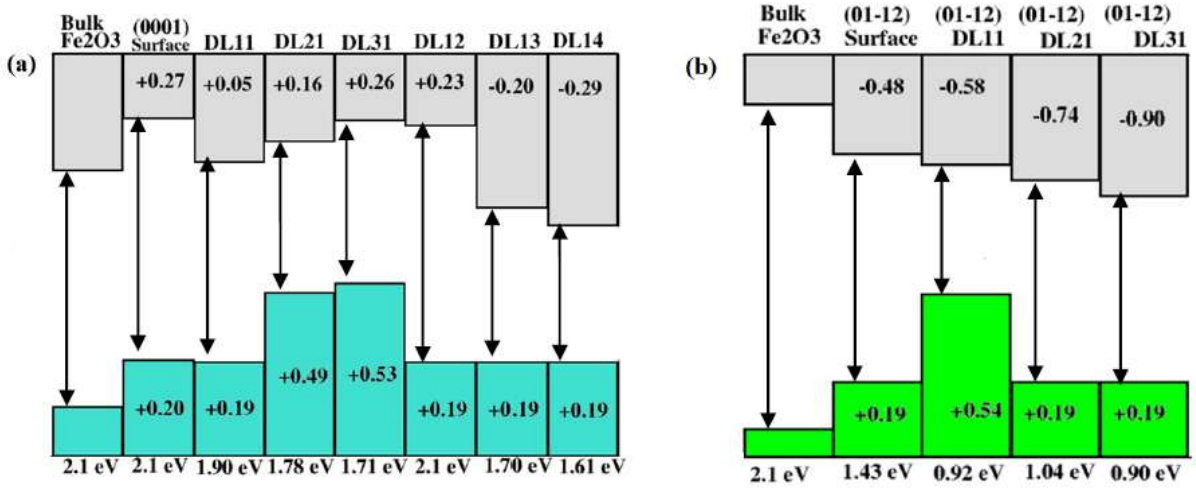

Fig. 7 Calculated band edge (VBM and CBM) positions of pure and Zn-doped surfaces of (a) {0001} surface (b) {01 $\bar{1}$ 2} as measured with respect to that of bulk α-Fe_2O_3. The plus (+) and minus (-) signs implies the up shift or down shift of the VBM or CBM with respect to the VBM and CBM of the bulk hematite respectively. DL11, DL21 and DL31 carry the same notation of different doping positions as explained earlier.

4. Conclusion

The influence of Zn atom on the electronic properties of {0001} and {01 $\bar{1}$ 2} surfaces of hematite for improved PEC water splitting has been studied from first-principles calculations. The doped systems were found to be thermodynamically stable and would prefer exothermic formation under oxygen rich conditions. It is found that even with mono-doping of Zn on the topmost layer L1 of the {0001} α-Fe_2O_3 surface, the band gap can be decreased without impurity states in the band structure which normally act as recombination centres. At the doping concentration of 4.20% of Zn atoms on L1 of {0001} surface, the CBM is shifted upwards by 0.23 eV as compared to the bulk. On the other hand with a single doping of Zn atom on the {01 $\bar{1}$ 2} surface the band gap is decreased, while the CBM of DL21 and DL31 become wavier and delocalised suggesting improved electron mobility of hematite surface. The charge density difference plots and the Bader charge analysis showed accumulation of charge on top of the surface, implying that the photo generated charge carriers can efficiently diffuse to the surface for enhanced interfacial charge transfer to the adsorbates. The observed features in our results: high accumulation of the electronic charges at the surface, the decrease in band gap and the absence of impurity states within the band structure and the up shift of CBM, suggest that mono-doping of Zn atom at the topmost layer L1 of {0001} surface can improve the photocatalytic activity of hematite for water splitting.

5. Acknowledgments

The authors acknowledge financial support from the Ministry of Higher Education (Zambia) through the Copperbelt University under the staff development fellowship. Further gratitude goes to the University of Pretoria and the Center for High Performance Computing (CHPC), Research Institute in Cape Town, South Africa for the cluster resources. AB and MD acknowledges financial support from the Swiss South African Joint Research Programme project "Production of Liquid Solar Fuels from CO_2 and water: Using Renewable Energy Resources" (IZLSZ2-149031). AB is grateful from the Swiss Nano Tera project SHINE (Solar Hydrogen Integrated Nano Electrolyzer, 20NA21-145936).

References

[1] A. Braun, E. Gaillard, E.L. Miller, H. Wang, Advanced materials and structures for solar fuels: introduction, J. Mater. Res, 31 (2016) 1545-1546.
[2] M. Barroso, S.R. Pendlebury, A.J. Cowan, J.R. Durrant, Charge carrier trapping, recombination and transfer in hematite (α-Fe 2 O 3) water splitting photoanodes, Chemical Science, 4 (2013) 2724-2734.
[3] P. Liao, J.A. Keith, E.A. Carter, Water oxidation on pure and doped hematite (0001) surfaces: Prediction of Co and Ni as effective dopants for electrocatalysis, Journal of the American Chemical Society, 134 (2012) 13296-13309.
[4] N. Mirbagheri, D. Wang, C. Peng, J. Wang, Q. Huang, C. Fan, E.E. Ferapontova, Visible light driven photoelectrochemical water oxidation by Zn-and Ti-doped hematite nanostructures, Acs Catalysis, 4 (2014) 2006-2015.
[5] Y.-S. Hu, A. Kleiman-Shwarsctein, G.D. Stucky, E.W. McFarland, Improved photoelectrochemical performance of Ti-doped α-Fe 2 O 3 thin films by surface modification with fluoride, Chemical Communications, (2009) 2652-2654.
[6] L. Xi, P.S. Bassi, S.Y. Chiam, W.F. Mak, P.D. Tran, J. Barber, J.S.C. Loo, L.H. Wong, Surface treatment of hematite photoanodes with zinc acetate for water oxidation, Nanoscale, 4 (2012) 4430-4433.
[7] Z. Chen, T.G. Deutsch, H.N. Dinh, K. Domen, K. Emery, A.J. Forman, N. Gaillard, R. Garland, C. Heske, T.F. Jaramillo, Experimental Considerations, Photoelectrochemical Water Splitting, Springer2013, pp. 17-44.
[8] J. Gan, X. Lu, Y. Tong, Towards highly efficient photoanodes: boosting sunlight-driven semiconductor nanomaterials for water oxidation, Nanoscale, 6 (2014) 7142-7164.
[9] H. Pan, X. Meng, G. Qin, Hydrogen generation by water splitting on hematite (0001) surfaces: first-principles calculations, Physical Chemistry Chemical Physics, 16 (2014) 25442-25448.
[10] J. Simfukwe, R.E. Mapasha, A. Braun, M. Diale, Density Functional Theory study of Cu doped {0001} and {01-1 2} surfaces of hematite for water splitting, MRS Advances, 3 (2018) 669-678.
[11] Y.W. Phuan, W.-J. Ong, M.N. Chong, J.D. Ocon, Prospects of electrochemically synthesized hematite photoanodes for photoelectrochemical water splitting: a review, Journal of Photochemistry and Photobiology C: Photochemistry Reviews, 33 (2017) 54-82.
[12] J.A. Glasscock, P.R. Barnes, I.C. Plumb, N. Savvides, Enhancement of photoelectrochemical hydrogen production from hematite thin films by the introduction of Ti and Si, The Journal of Physical Chemistry C, 111 (2007) 16477-16488.

[13] N.J. Cherepy, D.B. Liston, J.A. Lovejoy, H. Deng, J.Z. Zhang, Ultrafast studies of photoexcited electron dynamics in γ-and α-Fe2O3 semiconductor nanoparticles, The Journal of Physical Chemistry B, 102 (1998) 770-776.
[14] F. Le Formal, M. Grätzel, K. Sivula, Controlling photoactivity in ultrathin hematite films for solar water- splitting, Advanced Functional Materials, 20 (2010) 1099-1107.
[15] N. Seriani, Ab initio simulations of water splitting on hematite, Journal of Physics: Condensed Matter, 29 (2017) 463002.
[16] W.B. Ingler Jr, J.P. Baltrus, S.U. Khan, Photoresponse of p-type zinc-doped iron (III) oxide thin films, Journal of the American Chemical Society, 126 (2004) 10238-10239.
[17] A. Kleiman-Shwarsctein, M.N. Huda, A. Walsh, Y. Yan, G.D. Stucky, Y.-S. Hu, M.M. Al-Jassim, E.W. McFarland, Electrodeposited aluminum-doped α-Fe2O3 photoelectrodes: experiment and theory, Chemistry of Materials, 22 (2009) 510-517.
[18] S. Kumari, C. Tripathi, A.P. Singh, D. Chauhan, R. Shrivastav, S. Dass, V.R. Satsangi, Characterization of Zn-doped hematite thin films for photoelectrochemical splitting of water, Current Science (00113891), 91 (2006).
[19] H. Pan, X. Meng, D. Liu, S. Li, G. Qin, (Ti/Zr, N) codoped hematite for enhancing the photoelectrochemical activity of water splitting, Physical Chemistry Chemical Physics, 17 (2015) 22179-22186.
[20] K.J. McDonald, K.-S. Choi, Synthesis and photoelectrochemical properties of Fe2O3/ZnFe2O4 composite photoanodes for use in solar water oxidation, Chemistry of Materials, 23 (2011) 4863-4869.
[21] A.G. Tamirat, J. Rick, A.A. Dubale, W.-N. Sub, B.-J. Hwang, Using hematite for photoelectrochemical water splitting: a review of current progress and challenges.
[22] J. Wang, H. Sun, J. Huang, Q. Li, J. Yang, Band structure tuning of TiO2 for enhanced photoelectrochemical water splitting, The Journal of Physical Chemistry C, 118 (2014) 7451-7457.
[23] K. Nagaveni, M. Hegde, G. Madras, Structure and photocatalytic activity of Ti1-x M x O2±δ (M= W, V, Ce, Zr, Fe, and Cu) synthesized by solution combustion method, The Journal of Physical Chemistry B, 108 (2004) 20204-20212.
[24] S.-m. Chang, W.-s. Liu, Surface doping is more beneficial than bulk doping to the photocatalytic activity of vanadium-doped TiO2, Applied Catalysis B: Environmental, 101 (2011) 333-342.
[25] S. Kumari, A.P. Singh, C. Tripathi, D. Chauhan, S. Dass, R. Shrivastav, V. Gupta, K. Sreenivas, V.R. Satsangi, Enhanced photoelectrochemical response of Zn-dotted hematite, International Journal of Photoenergy, 2007 (2007).
[26] Y.-C. Chen, C.-L. Kuo, Y.-K. Hsu, Facile preparation of Zn-doped hematite thin film as photocathode for solar hydrogen generation, Journal of Alloys and Compounds, 768 (2018) 810-816.
[27] N. Snir, N. Yatom, M.C. Toroker, Progress in understanding hematite electrochemistry through computational modeling, Computational Materials Science, 160 (2019) 411-419.
[28] N. Dzade, A. Roldan, N. de Leeuw, A density functional theory study of the adsorption of benzene on hematite (α-Fe2O3) surfaces, Minerals, 4 (2014) 89-115.
[29] P. Giannozzi, S. Baroni, N. Bonini, M. Calandra, R. Car, C. Cavazzoni, D. Ceresoli, G.L. Chiarotti, M. Cococcioni, I. Dabo, QUANTUM ESPRESSO: a modular and open-source software project for quantum simulations of materials, Journal of physics: Condensed matter, 21 (2009) 395502.
[30] P. Hohenberg, W. Kohn, Inhomogeneous electron gas, Physical review, 136 (1964) B864.
[31] W. Kohn, L.J. Sham, Self-consistent equations including exchange and correlation effects, Physical review, 140 (1965) A1133.

[32] J.P. Perdew, K. Burke, M. Ernzerhof, Generalized gradient approximation made simple, Physical review letters, 77 (1996) 3865.
[33] R.S. Koster, C.M. Fang, M. Dijkstra, A. Van Blaaderen, M.A. Van Huis, Stabilization of rock salt ZnO nanocrystals by low-energy surfaces and Mg additions: a first-principles study, The Journal of Physical Chemistry C, 119 (2015) 5648-5656.
[34] S. Dudarev, G. Botton, S. Savrasov, C. Humphreys, A. Sutton, Electron-energy-loss spectra and the structural stability of nickel oxide: An LSDA+ U study, Physical Review B, 57 (1998) 1505.
[35] S. Dudarev, A. Liechtenstein, M. Castell, G. Briggs, A. Sutton, Surface states on NiO (100) and the origin of the contrast reversal in atomically resolved scanning tunneling microscope images, Physical Review B, 56 (1997) 4900.
[36] A. Liechtenstein, V. Anisimov, J. Zaanen, Density-functional theory and strong interactions: Orbital ordering in Mott-Hubbard insulators, Physical Review B, 52 (1995) R5467.
[37] A. Rohrbach, J. Hafner, G. Kresse, Ab initio study of the (0001) surfaces of hematite and chromia: Influence of strong electronic correlations, Physical Review B, 70 (2004) 125426.
[38] A. Bandyopadhyay, J. Velev, W. Butler, S.K. Sarker, O. Bengone, Effect of electron correlations on the electronic and magnetic structure of Ti-doped α-hematite, Physical Review B, 69 (2004) 174429.
[39] H.J. Monkhorst, J.D. Pack, Special points for Brillouin-zone integrations, Physical review B, 13 (1976) 5188.
[40] T.P. Trainor, A.M. Chaka, P.J. Eng, M. Newville, G.A. Waychunas, J.G. Catalano, G.E. Brown Jr, Structure and reactivity of the hydrated hematite (0 0 0 1) surface, Surface Science, 573 (2004) 204-224.
[41] W. Huang, R. Sun, J. Tao, L. Menard, R.G. Nuzzo, J.-M. Zuo, Coordination-dependent surface atomic contraction in nanocrystals revealed by coherent diffraction, Nature materials, 7 (2008) 308.
[42] W. Qi, B. Huang, M. Wang, Bond-length and-energy variation of small gold nanoparticles, Journal of Computational and Theoretical Nanoscience, 6 (2009) 635-639.
[43] C.Q. Sun, Size dependence of nanostructures: Impact of bond order deficiency, Progress in solid state chemistry, 35 (2007) 1-159.
[44] Z. Zhou, P. Huo, L. Guo, O.V. Prezhdo, Understanding hematite doping with group IV elements: a DFT+ U study, The Journal of Physical Chemistry C, 119 (2015) 26303-26310.
[45] H. Pan, B. Gu, G. Eres, Z. Zhang, Ab initio study on noncompensated CrO codoping of GaN for enhanced solar energy conversion, The Journal of chemical physics, 132 (2010) 104501.
[46] H. Li, Y. Guo, J. Robertson, Calculation of TiO2 surface and subsurface oxygen vacancy by the screened exchange functional, The Journal of Physical Chemistry C, 119 (2015) 18160-18166.